Chinese J. of Chem. Eng., 5(2) 105－116 (1997)

NUMERICAL SOLUTION OF VISCOUS FLOW PAST A SOLID SPHERE WITH THE CONTROL VOLUME FORMULATION*

Mao Zaisha(毛在砂)and Chen Jiayong(陈家镛)**

Institute of Chemical Metallurgy, Academia Sinica, Beijing 100080, China

Abstract The control volume formulation with the QUICK finite difference scheme is used to solve incompressible liquid flow past a solid sphere in terms of stream function and vorticity. Several technical points are addressed on improving the accuracy and efficiency of numerical simulation of similar problems of fluid flow. In particular, the importance of suitable specification of the distortion function to enforcing the far field boundary conditions is emphasized.

Keywords sphere, laminar flow, numerical simulation, control volume formulation, QUICK scheme

1 INTRODUCTION

The motion of a single particle (drop, bubble, or solid particle) or a swarm of particles in a fluid medium is of extreme significance to many academic topics and in industrial applications. In addition to theoretical and experimental investigations, numerical simulation has been extensively and effectively employed to promote our understanding of fluid mechanics related to the motion of a single particle, because analytical solution is available only in very limited occasions. Analytical solution of fluid flow around a solid or fluid sphere in creeping flow has been available decades ago[1]. For the case with $Re>1$ and for nonspherical solid particles, boundary layer approach, computational fluid dynamic approach and experimental investigation were equally popular tools for acquiring in-depth knowledge, and great progress has been achieved in this area to date. LeClair *et al.*[2], Rivkind & Ryskin[3], Ryskin and Leal[4], and Dandy and Leal[5] extended the numerical approach to the motion of bubbles and fluid drops. Nowadays, computational fluid flow and heat, mass transfer has become a useful and sophisticated technique.

To solve the external flow outside a solid sphere in an unbounded liquid medium, several approaches are available for the choice of an investigator. The Navier-Stokes equations are explicitly formulated in terms of primitive dependent variables (u and p), and can be solved directly for velocity and pressure fields as in many numerical studies, particularly for turbulent flows. However, in the intermediate range of the Reynolds number but still under the laminar conditions, two-dimensional Navier-Stokes equations may be presented in terms of two scalar variables, stream function and vorticity (ψ and ω). In general, a boundary-fitted orthogonal coordinate system is very

Received 1996－01－25, accepted 1996－05－02.

*Supported by the National Natural Science Foundation of China.

**To whom correspondence should be addressed.

efficient in dealing with evolution of free interface and whenever good accuracy is desired in enforcing the boundary conditions. In this respect, Ryskin and Leal provided very flexible strong constraint and weak constraint methods to generate the grid numerically for solving such flows[6].

As part of a long-term project on the mass transfer in multi-dispersed systems, the fluid flow around a solid sphere was numerically simulated based on a similar approach to that by Leal's group. In this course, several technical difficulties were brought to the authors' attention, which were analyzed and overcome in the course of compiling a computer code and validating it. Thus improved algorithm produced good prediction in accordance with the experimental data. In this paper, these experiences are addressed and discussed with an intention to benefit the numerical simulation of motion of bubbles and drops under the similar occasions.

2 MATHEMATICAL FORMULATION

2.1 Orthogonal boundary-fitted coordinate system

In this work, the numerical procedures for grid generation and solution of fluid mechanics equations are mainly adopted from what Ryskin and Leal[4], Dandy and Leal[5] described for the cases of deformable bubbles and drops. For a solid particle, only the infinite exterior domain needs to be solved. If a point in the physical domain is denoted as (x, y, θ) in the cylindrical coordinates, with θ being the azimuthal angle measured about the axis of symmetry, x-axis, this coordinate system can be transformed into a boundary-fitted orthogonal coordinate system (ξ, η, θ). The axisymmetry of the particle shape guarantees the mapping to be carried out over a half plane region $(-\infty < x < +\infty, y \geqslant 0)$ since the rotation of the resulting coordinate system (ξ, η) about the symmetric axis x will yield three-dimensional orthogonal boundary-fitted coordinates (ξ, η, θ). The mapping functions $x(\xi, \eta)$ and $y(\xi, \eta)$ can be solved from the covariant Laplace equations

$$\frac{\partial}{\partial \xi}\left(f \frac{\partial x}{\partial \xi}\right)+\frac{\partial}{\partial \eta}\left(\frac{1}{f} \frac{\partial x}{\partial \eta}\right)=0 \qquad \frac{\partial}{\partial \xi}\left(f \frac{\partial y}{\partial \xi}\right)+\frac{\partial}{\partial \eta}\left(\frac{1}{f} \frac{\partial y}{\partial \eta}\right)=0 \tag{1}$$

The condition of orthogonality leads to

$$\frac{\partial x}{\partial \eta}=-f \frac{\partial y}{\partial \xi} \qquad \frac{\partial y}{\partial \eta}=f \frac{\partial x}{\partial \xi} \tag{2}$$

which must also be satisfied on the boundary of the transformed region. In Eqs.(1) and (2) the distortion function $f(\xi, \eta)$ as termed by Ryskin and Leal[6] is the ratio of the scale factors

$$f(\xi, \eta)=h_\eta / h_\xi \tag{3}$$

where

$$h_\xi^2=\left(\frac{\partial x}{\partial \xi}\right)^2+\left(\frac{\partial y}{\partial \xi}\right)^2 \qquad h_\eta^2=\left(\frac{\partial x}{\partial \eta}\right)^2+\left(\frac{\partial y}{\partial \eta}\right)^2 \tag{4}$$

The distortion function measures the ratio of the sides of a small cell on the x-y

plane which is an image of a small square on the ξ-η plane. By judicious choice of the distortion function, the density distribution of computational grids in the x-y plane may be controlled so as to achieve faster convergence and better accuracy in numerical solution.

The mapping is defined such that the solution domain (for any arbitrary fixed θ) is a unit square

$$0 \leqslant \xi,\ \eta \leqslant 1$$

but the resulted (ξ, η, θ) coordinate system is left-handed. The correspondence of the boundaries between the infinite exterior region and the transformed region is sketched in Fig. 1, with $\xi=1$ being the solid surface ($r=R$), $\xi=0$ corresponding to "infinity" approximated by a large circle with the radius equal to $r=\Lambda R$ ($\Lambda=20$ being large enough), and η varying from 0 to 1 as a point is traversed along the solid surface from the rear stagnant point A to the front stagnancy C in Fig.1(a). If $f(\xi, \eta)$ is specified and fixed, the value of Λ may be determined in the course of numerical grid generation by solving Eq.(1). Note that when later solving the nondimensional equation of liquid flow, the drop radius is normalized to unity and the computational domain extends to Λ in the radial direction.

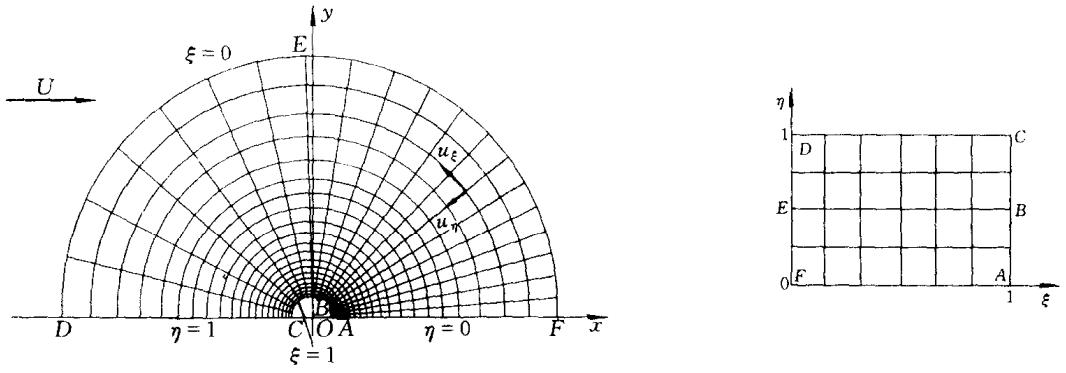

(a) The computational grid in the x-y plane (b) The transformed domain in the ξ-η plane

Figure 1 Sketch of the computational domain exterior to a solid sphere and the mapping to the transformed ξ-η plane (The correspondence between two domains is indicated by the capital letters A through F)

The orthogonal mapping by the numerical solution of Eq.(1) is subject to the following boundary conditions

$$\frac{\partial x}{\partial \eta}=0,\ y=0,\ \text{at}\ \eta=0\ \text{ or }\ \eta=1 \tag{5}$$

$$f\frac{\partial x}{\partial \xi}=\frac{\partial y}{\partial \eta},\ \frac{\partial x}{\partial \eta}=-f\frac{\partial y}{\partial \xi},\ \text{at}\ \xi=0\ \text{ or }\ \xi=1 \tag{6}$$

The orthogonal conditions (6) mean that if the distortion function $f(\xi, \eta)$ is specified explicitly throughout the ξ-η region, both $x(1, \eta)$ and $y(1, \eta)$, which represent a

prescribed distribution of grid points along the boundary $\xi=1$, can not be given simultaneously. In the case of a solid sphere, orthogonality simply indicates that the boundary nodes are right on the radial straight lines from the center of the sphere passing through its nearest neighboring node. However, the orthogonal coordinate system may be specified analytically without resorting to solving the partial differential equations numerically in some simple cases, as exemplified later in Section 3.3.

2.2 Formulation of fluid flow

Suppose a solid sphere moving under gravity at its terminal velocity U in a quiescent fluid (density ρ and viscosity μ), which is assumed to be incompressible and Newtonian. In addition, attention is focused on steady, isothermal, laminar and axisymmetric flow which is physically realistic under controlled experimental conditions.

By taking the uniform velocity U at upstream infinity along the direction of x-axis as the characteristic velocity, and the radius of the sphere R as the characteristic length, the Navier-Stokes equations can be written in terms of stream function ψ and vorticity ω and in dimensionless form as

$$L^2(y\omega)-\frac{Re}{2}\frac{1}{h_\xi h_\eta}\left[\frac{\partial\psi}{\partial\xi}\frac{\partial}{\partial\eta}\left(\frac{\omega}{y}\right)-\frac{\partial\psi}{\partial\eta}\frac{\partial}{\partial\xi}\left(\frac{\omega}{y}\right)\right]=0 \tag{7}$$

$$L^2\psi+\omega=0 \tag{8}$$

where the differential operator is

$$L^2=\frac{1}{h_\xi h_\eta}\left[\frac{\partial}{\partial\xi}\left(\frac{f}{y}\frac{\partial}{\partial\xi}\right)+\frac{\partial}{\partial\eta}\left(\frac{1}{fy}\frac{\partial}{\partial\eta}\right)\right] \tag{9}$$

$Re=2UR\rho/\mu$ is the Reynolds number based on the physical properties of the liquid phase. The velocity components, as the auxiliary variables, are related to the stream functions by

$$u_\xi=-\frac{1}{yh_\eta}\frac{\partial\psi}{\partial\eta},\quad u_\eta=\frac{1}{yh_\xi}\frac{\partial\psi}{\partial\xi} \tag{10}$$

in this left-hand coordinate system. To solve the vorticity equation by the control volume formulation, it is convenient to work with a new variable $\omega^*=y\omega$ instead of the original ω. Eq.(7) is further manipulated to

$$L^2(\omega^*)=\frac{Re}{2}\frac{1}{h_\xi h_\eta}\left[\frac{\partial}{\partial\xi}\left(-\frac{\partial\psi}{\partial\eta}\frac{\omega^*}{y^2}\right)+\frac{\partial}{\partial\eta}\left(\frac{\partial\psi}{\partial\xi}\frac{\omega^*}{y^2}\right)\right] \tag{11}$$

by making use of the following relationships

$$\frac{\partial\psi}{\partial\xi}\frac{\partial}{\partial\eta}\left(\frac{\omega^*}{y^2}\right)=\frac{\partial}{\partial\eta}\left(\frac{\partial\psi}{\partial\xi}\frac{\omega^*}{y^2}\right)-\frac{\omega^*}{y^2}\frac{\partial^2\psi}{\partial\xi\partial\eta}$$

$$\frac{\partial\psi}{\partial\eta}\frac{\partial}{\partial\xi}\left(\frac{\omega^*}{y^2}\right)=\frac{\partial}{\partial\xi}\left(\frac{\partial\psi}{\partial\eta}\frac{\omega^*}{y^2}\right)-\frac{\omega^*}{y^2}\frac{\partial^2\psi}{\partial\xi\partial\eta}$$

The control volume formulation is more suitable for solving Eq.(11) when both sides

are multiplied by $h_\xi h_\eta$, and Eq.(11) is integrated separately over control volumes when being discretized. The dimensionless variables and the operator are related to its dimensional counterpart as follows

$$\omega' = (U/R)\omega,\ \psi' = R^2 U\psi,\ L'^2 = (1/R^3)L^2$$

The governing equations of fluid dynamics are subject to the following boundary conditions. At the symmetry axis

$$\psi = 0,\ \omega = 0 \quad \text{at } \eta = 0,\ 1 \tag{12}$$

The far-field boundary conditions representing undisturbed parallel flow outside the sphere are

$$\psi \to (1/2)y^2,\quad \omega \to 0 \quad \text{for} \quad \xi \to 0 \tag{13}$$

At the solid surface ($\xi = 1$)

$$\psi = 0 \tag{14}$$

corresponds to zero normal velocity. In addition, the boundary value $\omega(1, \eta)$ is also needed, which should be evaluated from the no-slip condition on the solid surface

$$u_\eta = 0 \tag{15}$$

Once the fields of ψ and ω are solved, other flow properties can be calculated as described by Dandy and Leal[5]. The drag coefficient defined by

$$C_D = 2\ (\text{drag force})/(\rho U^2 \pi R^2)$$

can be calculated by integration along the solid surface

$$C_D = 2\int_0^1 (\tau_{\xi\xi}\frac{\partial y}{\partial \eta} - \tau_{\xi\eta}\frac{\partial x}{\partial \eta})y\mathrm{d}\eta \tag{16}$$

with

$$\tau_{\xi\xi} = \frac{4}{Re}\int_0^\eta \frac{f}{y}\frac{\partial}{\partial \xi}(y\omega)\mathrm{d}\eta \tag{17}$$

$$\tau_{\xi\eta} = -(4/Re)\omega \tag{18}$$

2.3 The QUICK differencing scheme

The Power-Law Differencing Scheme suggested by Patankar is an efficient and numerically stable one[7]. However, as the cell Peclet number increases, the scheme shifts automatically toward the Upwind Differencing Scheme with first-order accuracy. It is desired to incorporate a second-order scheme in the control volume formulation. For this purpose, the QUICK scheme with quadratic interpolation on convective terms was adopted in the present work. QUICK was first proposed by Leonard[8] and successfully used by many investigators[9-11]. This scheme is also used here to achieve second-order accuracy of the solution.

Discretization of Eq.(11) can be exemplified with a general differential equation such as

$$\frac{\partial}{\partial\xi}(\Gamma\frac{\partial\phi}{\partial\xi})+\frac{\partial}{\partial\eta}(\Gamma\frac{\partial\phi}{\partial\eta})=\frac{\partial}{\partial\xi}(u_\xi\phi)+\frac{\partial}{\partial\eta}(u_\eta\phi) \tag{19}$$

integration of Eq.(19) can be carried out over a control cell to give

$$\Gamma_e\frac{\Delta\eta}{\Delta\xi}(\phi_E-\phi_P)-\Gamma_w\frac{\Delta\eta}{\Delta\xi}(\phi_P-\phi_W)+\Gamma_n\frac{\Delta\xi}{\Delta\eta}(\phi_N-\phi_P)-\Gamma_s\frac{\Delta\xi}{\Delta\eta}(\phi_P-\phi_S)=$$

$$(u_{\xi e}\phi_e-u_{\xi w}\phi_w)\Delta\eta+(u_{\eta n}\phi_n-u_{\eta s}\phi_s)\Delta\xi \tag{20}$$

in which the capital letter subscripts (N, S, E, W) denote the position of neighboring nodes and the lower-case letter subscripts (n, s, e, w) mark the cell faces as indicated in Fig.2 (a). It is possible to use upwind quadratic interpolation to get a second-order estimation of velocity components at the cell faces, and this leads to

$$\phi_w=(\alpha_{-2}\phi_{WW}+\alpha_{-1}\phi_W+\alpha_0\phi_P+\alpha_1\phi_E)\ M_w^+ +(\beta_{-2}\phi_{WW}+\beta_{-1}\phi_W+\beta_0\phi_P+\beta_1\phi_E)\ M_w^- \tag{21}$$

$$\phi_e=(\gamma_{-1}\phi_W+\gamma_0\phi_P+\gamma_1\phi_E+\gamma_2\phi_{EE})M_e^+ +(\delta_{-1}\phi_W+\delta_0\phi_P+\delta_1\phi_E+\delta_2\phi_{EE})M_e^- \tag{22}$$

$$\phi_s=(\alpha_{-2}\phi_{SS}+\alpha_{-1}\phi_S+\alpha_0\phi_P+\alpha_1\phi_N)M_s^+ +(\beta_{-2}\phi_{SS}+\beta_{-1}\phi_S+\beta_0\phi_P+\beta_1\phi_N)\ M_s^- \tag{23}$$

$$\phi_n=(\gamma_{-1}\phi_S+\gamma_0\phi_P+\gamma_1\phi_N+\gamma_2\phi_{NN})M_n^+ +(\delta_{-1}\phi_S+\delta_0\phi_P+\delta_1\phi_N+\delta_2\phi_{NN})M_n^- \tag{24}$$

with

$$M_i^+=(u_{\xi i}+|u_{\xi i}|)/2u_{\xi i},\ M_i^-=(u_{\xi i}-|u_{\xi i}|)/2u_{\xi i},\ i=\omega,\ e$$

$$M_j^+=(u_{\eta j}+|u_{\eta j}|)/2u_{\eta j},\ M_j^-=(u_{\eta j}-|u_{\eta j}|)/2u_{\eta j},\ j=s,\ n$$

deciding which three upwind nodes to be chosen for the quadratic interpolation of ϕ's. Denoting

$$D_e=\Gamma_e(\Delta\eta/\Delta\xi),\ D_w=\Gamma_w(\Delta\eta/\Delta\xi),\ D_n=\Gamma_n(\Delta\xi/\Delta\eta),\ D_s=\Gamma_s(\Delta\xi/\Delta\eta),$$

$$C_e=u_{\xi e}\Delta\eta,\ C_w=u_{\xi w}\Delta\eta,\ C_n=u_{\eta n}\Delta\xi,\ C_s=u_{\eta s}\Delta\xi,$$

the following discretized equation is resulted

$$a_P\phi_P=a_W\phi_W+a_E\phi_E+a_S\phi_S+a_N\phi_N+S_P$$

with

$$a_P=(D_e+D_w+D_n+D_s)+C_e(\gamma_0M_e^+ +\delta_0M_e^-)-C_w(\alpha_0M_w^+ +\beta_0M_w^-)$$
$$+C_n(\gamma_0M_n^+ +\delta_0M_n^-)-C_s(\alpha_0M_s^+ +\beta_0M_s^-)$$
$$a_W=D_w+(\alpha_{-1}M_w^+ +\beta_{-1}M_w^-)C_w-(\gamma_{-1}M_e^+ +\delta_{-1}M_e^-)C_e$$
$$a_E=D_e+(\alpha_1M_w^+ +\beta_1M_w^-)C_w-(\gamma_1M_e^+ +\delta_1M_e^-)C_e$$
$$a_S=D_s+(\alpha_{-1}M_s^+ +\beta_{-1}M_s^-)C_s-(\gamma_{-1}M_n^+ +\delta_{-1}M_n^-)C_n$$
$$a_N=D_n+(\alpha_1M_s^+ +\beta_1M_s^-)C_s-(\gamma_1M_n^+ +\delta_1M_n^-)C_n$$
$$S_P=(\alpha_{-2}M_w^+ +\beta_{-2}M_w^-)C_w\phi_{WW}-(\gamma_2M_e^+ +\delta_2M_e^-)C_e\phi_{EE}$$
$$+(\alpha_{-2}M_s^+ +\beta_{-2}M_s^-)C_s\phi_{SS}-(\gamma_2M_n^+ +\delta_2M_n^-)C_n\phi_{NN}$$

Since the uniform grid in the (ξ, η) plane is used, the interpolation coefficients are

simple constants as listed in Fig.2(b). With suitable relaxation to make the diagonal elements in the coefficient matrix of the algebraic equation set dominant in magnitude and sufficient number of meshes, convergence of the above discretized equations is well guaranteed.

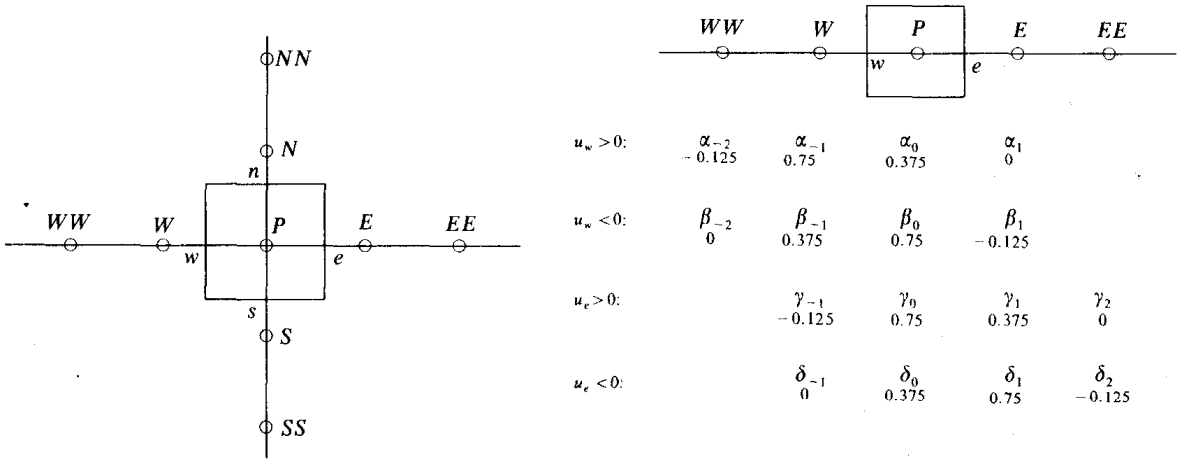

(a) The control volume and its neighbor nodes (b) Interpolation for faces w and e uses different sets of coefficients while two upwind nodes are always utilized

Figure 2 The control volume and the coefficient sets for the second-order accurate interpolation of ϕ values at the cell faces

2.4 Solution algorithm

The numerical procedure consists of the following steps

(1) Generation of the orthogonal grid numerically or analytically specifying the distortion function $f(\xi, \eta)$, $x(\xi, \eta)$ and $y(\xi, \eta)$, and then initialization of the fields, including all the auxiliary variables and scaling factors.

(2) Discretize Eqs.(8) and (11) by the Power-Law Scheme as described by Patankar[7] or the QUICK scheme outlined in the previous section.

(3) Solve successively the stream function and vorticity equations Eqs.(8) and (11), subject to the boundary conditions (12) through (15).

(4) Implementation of boundary condition (15) may be done iteratively

$$[\omega^*(1, \eta)]^{\{n+1\}} = [\omega^*(1, \eta)]^{\{n\}} + c_1 u_\eta(1, \eta)^{\{n\}} \tag{25}$$

where n denotes the iteration number and c_1 is a specified constant.

(5) Repeat steps 3 and 4 till convergence [average deviation of Eq.(15) below 10^{-5}].

3 NUMERICAL RESULTS AND DISCUSSION

3.1 Modification of the infinite boundary condition

A modification to remove the infinite boundary condition for ψ as $\xi \to 0$ [Eq.(15)] was adopted by Ryskin and Leal [4]. The modified stream function

$$\psi^* \equiv \psi - (1/2)y^2(1-\xi^3)$$

would result in $\psi^*=0$ for $\xi=0$ and maintains the homogeneous boundary conditions on the other three boundaries. The term $y^2(1-\xi^3)/2$ is the potential flow solution for a spherical bubble, but it has no simple physical meaning for the viscous flow outside a solid sphere. When ψ^* and ω are finally solved, ψ^* is then converted to ψ for further

calculation of C_D and other hydrodynamic parameters. However, Eq. (11) demands calculating the derivatives of the original stream function numerically in each iteration. This operation involves differentiation of the term $y^2(1-\xi^3)/2$ and would introduce additional numerical error to the discretized equations of ω if ψ^* is used. In this work, we choose to solve the ψ equation in its original form when investigating the dependence of flow on the Reynolds number. However, the results of numerical experiments in section 3.3 suggest that the solution in terms of ψ or ψ^* is equally acceptable.

3.2 Boundary conditions at far downstream

The boundary conditions for ψ and ω at the far downstream require attention from the view point of computational accuracy and efficiency. For a solid sphere with intermediate Reynolds number, the vorticity is created in the neighborhood of the sphere and transported downstream by liquid convection. If the solution domain is truncated at the outer computational radius where the vorticity is not heavily dissipated, enforcing the zero vorticity condition is hardly justified. On the other hand, the vorticity at far downstream presents only very weak effect on the recirculating wake, and it is not economic to use a large computational domain just for minor improvement in computational accuracy. As a compromise, it seems acceptable to use the condition of zero derivative in the flow direction to replace the Dirichlet boundary condition. With $\partial\phi/\partial x=0$, the boundary value of stream function or vorticity can be simply designated with the upstream one from interpolation as sketched in Fig.3.

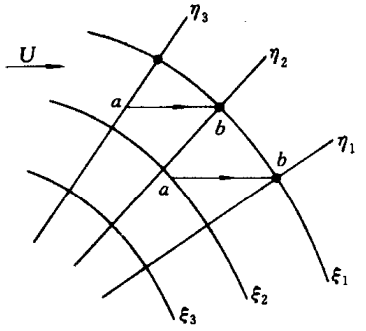

Figure 3 Scheme for implementing the downstream boundary conditions of zero derivative at the outer computational border ($\xi_1=0$)

The value of ϕ at point a obtained from linear interpolation is designated to node b

3.3 Suitable specification of distortion function

In this work, the distortion function is specified as

$$f(\xi,\ \eta)=(\pi/\lambda)\ (1-0.5\cos\pi\eta) \tag{26}$$

which offers small values for η in the lower range (near the trailing stagnant point) where more grid lines are desired to be allocated for better numerical resolution of a possible recirculating wake. For this specification and a spherical particle, the orthogonal transform is found in the analytical form of

$$\begin{cases} x=\exp[\lambda(1-\xi)]\cos(\pi\eta-0.5\ \sin\pi\eta) \\ y=\exp[\lambda(1-\xi)]\sin(\pi\eta-0.5\ \sin\pi\eta) \end{cases} \tag{27}$$

The factor λ indicates the speed of increase for the spacing between two adjacent constant-ξ lines, and f is maintained at finite level since the spacing in two coordinate direction increases synchronously. Fig.1(a) depicts such an orthogonal coordinate system

around a spherical particle.

Ryskin and Leal[4] suggested another specification of the distortion function

$$f(\xi, \eta)=\pi\xi(1-0.5\ \cos\pi\eta) \tag{28}$$

for both the flow field and an auxiliary domain. The latter was essentially the half circle in the X-Y plane, and then used a conformal mapping

$$x-iy=1/(X+iY) \tag{29}$$

to transform the half circle into the infinite region in the x-y plane[6]. That is to transform the analytical orthogonal grid system

$$\begin{cases} X=\xi\cos(\pi\eta-0.5\sin\pi\eta) \\ Y=\xi\sin(\pi\eta-0.5\sin\pi\eta) \end{cases} \tag{30}$$

into the computational grids with specified distortion function Eq.(28) intact. This transform had the advantage that the nodes with $\xi=0$ were at the "real" infinity where the grid density became vanishingly low as one may intuitively incline to have.

However, this distortion function may not be suitable for effectively enforcing the boundary value of ψ as prescribed by Eq.(13). Upon discretization according to the control volume formulation[7], Eq.(8) multiplied by $h_\xi h_\eta$ will result in

$$a_P\psi_P=a_W\psi_W+a_E\psi_E+a_S\psi_S+a_N\psi_N+h_\xi h_\eta\omega_P\Delta\xi\Delta\eta \tag{31}$$

with

$$a_P=a_W+a_E+a_S+a_N$$

$$a_W=\frac{f}{y}\bigg|_w\frac{\Delta\eta}{\Delta\xi},\quad a_E=\frac{f}{y}\bigg|_e\frac{\Delta\eta}{\Delta\xi},\quad a_S=\frac{1}{fy}\bigg|_s\frac{\Delta\xi}{\Delta\eta},\quad a_N=\frac{1}{fy}\bigg|_n\frac{\Delta\xi}{\Delta\eta}$$

As Eq.(28) gives very small value of $f(\xi, \eta)$ near $\xi=0$ (in the far field), the coefficients a_W and a_E become rather small as compared with a_S and a_N. In the limit Eq.(31) becomes

$$a_P\psi_P\approx a_S\psi_S+a_N\psi_N+h_\xi h_\eta\omega_P\Delta\xi\Delta\eta \tag{32}$$

and this in turn means a Newmann boundary condition of zero derivative of ψ in the ξ-direction would be enforced instead of the original Dirichlet boundary condition at the outer computational radius. In fact, from the comparison among the computational results on a 41×41 grid listed in Table 1 it is observed that only the distortion function Eq. (26) generates reasonable results on the drag coefficients and length of recirculation zone behind the sphere, L_w. It is also noticed that modifying ψ or adopting either Dirichlet or Newmann downstream boundary conditions play only a minor role in our case of numerical simulation.

Reviewing earlier literatures on flow past a sphere, it is noticed that many authors adopted the uniform grid in the transformed polar coordinate system ($\ln r$, ϕ), so that the mesh size Δr in the radial direction grows exponentially to match the increasing $r\Delta\phi$ in the far flow field[12-14]. Thus, finite values of the distortion function were established throughout the flow domain.

Table 1 Comparison of C_D and L_w from simulation and literature data

($Re=50$, QUICK scheme, 41×41 grid)

Downstream B. C.		Distortion function	ψ modified?	C_D	L_w
Literature data				1.574	0.42
Simulated results	Dirichlet B. C.	Eq.(26)	No	1.5529	0.3798
		Eq.(26)	Yes	1.5472	0.4106
		Eq.(28)	No	1.9173	0.4902
		Eq.(28)	Yes	1.9865	0.5861
	$\frac{\partial}{\partial x}=0$	Eq.(26)	No	1.5497	0.3855
		Eq.(26)	Yes	1.5435	0.4166
		Eq.(28)	No	2.0848	0.4545
		Eq.(28)	Yes	2.1195	0.5360

3.4 Validation of the numerical scheme

The computational results on the drag coefficient and the wake length for a sphere with $Re=50$ using two differencing schemes on a series of computational grids (41×41, 61×61, 81×81, 101×101, and 121×121) indicate that the Power-Law Difference scheme is roughly of first order accuracy as obviously suggested by the linearity of the predicted L_w against the mesh size used, $\Delta\xi$(Fig.4). On the contrary, the QUICK scheme shows apparent superiority in the order of accuracy. As the grid is refined from 61×61 to 121×121, the predicted C_D is only changed by 1.0% and L_w is increased by 1.2%. Therefore, a 81×81 grid and the QUICK scheme are used in latter simulations.

Simulation of a solid sphere in unbounded quiescent liquid was performed for the cases with $Re=50$, 100, and 200. Fig.5 presents the stream line maps of these cases. The numerical results of C_D and L_w were compared with typical literature data. Table 2 is the comparison on the drag coefficient, and its coincidence to the values of C_D calculated from a correlation for the range of Re from 20 to 200 as recommended by Clift *et al.* (page 112 in Ref.[1]) is quite reasonable. Comparison of the length of the wake is shown in Fig.6, where our numerical results are compared with the experimental results by Taneda[15], and the agreement seems satisfactory. For the cases of $Re=$ 150 and 200, the prediction deviates from the trend of experimental data, and the possible reason is that the real wake becomes oscillatory while the numerical simulation was based on the assumption of a steady wake.

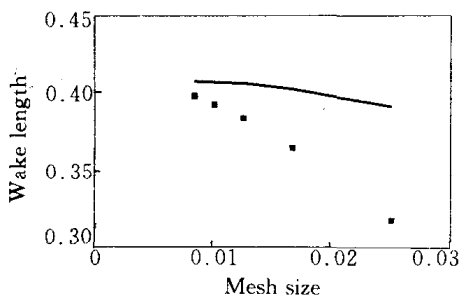

Figure 4 Grid dependence of computed wake length on the discretizing schemes with different orders of accuracy

— QUICK scheme; ■ Power-law scheme

4 CONCLUSIONS

(1) Numerical solution of the motion of a solid sphere with the stream func-

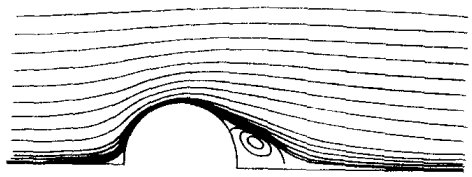

(a) $Re=50$

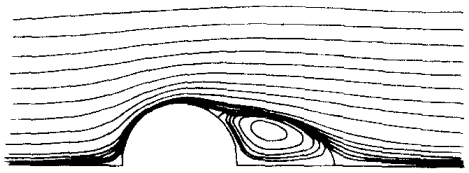

(b) $Re=100$

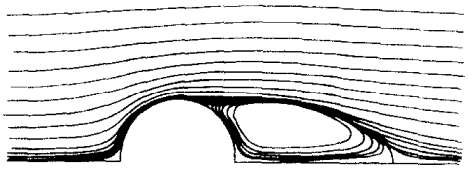

(c) $Re=200$

Figure 5 Streamline contour maps for viscous flow past a solid sphere (81×81 grid, QUICK scheme, downstream zero derivative)

Table 2 Comparison of C_D from simulation and available correlation

(in ψ, distortion function Eq.(26), downstream zero derivative, QUICK scheme, 81×81 grid)

Re	This work	Correlation
20	2.696	2.735
50	1.564	1.574
100	1.087	1.085
150	0.896	0.889
200	0.787	0.776

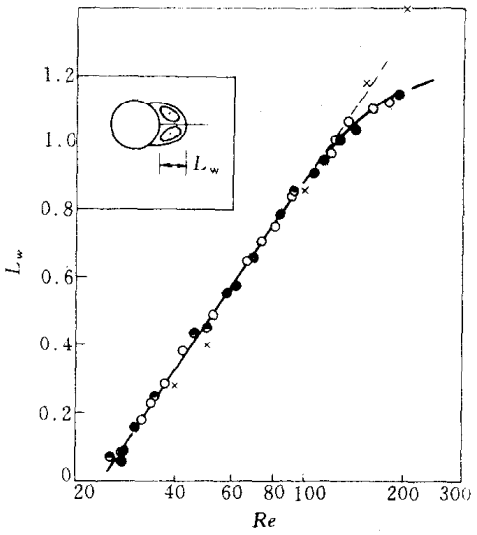

Figure 6 Comparison of predicted wake length with experimental data[15] ($Re=Ud\rho/\mu$)

○ ● ◓ experimental data[15]; × this work

d/mm: ○ 19.82; ● 15.08; ◓ 9.52

tion-vorticity formulation is confirmed to be efficient for laminar viscous flow when the inertia term is not negligible (in the intermediate range of Re). Eq.(11) is found to be a more suitable form for solution with the control volume formulation. It seems that there is no need to modify the stream function in order to obtain homogeneous boundary conditions at the outer computational radius.

(2) Suitable choice of the computational grid, including that in the far flow field, is of critical importance for accurate solution of the fluid flow and correct enforcement of the far field boundary conditions. The proposed distortion function Eq.(26) maintains to be the order of unity in the far flow field is proved to be advantageous to higher computational precision.

(3) It is confirmed that second-order QUICK scheme is more accurate than the popular Power-Law Scheme which degenerates to first-order accuracy as Re is increased. It seems that the QUICK scheme is easy to be implemented for a uniform grid, which is often the case when a boundary-fitted coordinate system is adopted.

ACKNOWLEDGEMENTS

The authors thank Dr. Sun Changgui for providing the FORTRAN source program from which the current version of computer codes is developed.

NOMENCLATURE

a	coefficient of discretized equation
C_D	drag coefficient
$f(\xi, \eta)$	distortion function
h	scale factor
L	differential operator
L_w	wake length measured with spherical diameter
n	iteration number
R	drop radius, m
Re	Reynolds number ($Re=2UR\rho/\mu$)
r	radial coordinate, m
U	far field flow velocity, $m \cdot s^{-1}$
u	nondimensional local velocity
X, Y	Cartesian coordinates in auxiliary plane
x, y	nondimensional Cartesian coordinates
$\alpha, \beta, \gamma, \delta$	interpolation coefficient
Γ	general diffusivity for ϕ
θ	azimuthal coordinate
λ	constant in Eq.(26)
μ	viscosity, $N \cdot s \cdot m^{-2}$
ξ, η	transformed boundary-fitted coordinates
ρ	density, $kg \cdot m^{-3}$
τ	nondimensional stress tensor
ϕ	general physical variable
ψ	stream function
ω	vorticity

REFERENCES

1 Clift, R., Grace, J. R. and Weber, M. E., Bubbles, Drops and Particles, Academic Press, New York (1978).
2 LeClair, B. P., Hamielec, A. E., Pruppacher, H. R. and Hall, W. D., *J. Atmos. Sci.*, **29**, 728(1972).
3 Rivkind, V. Y. and Ryskin, G., *Fluid Dyn.*, **11**, 5(1976).
4 Ryskin, G. and Leal, L. G., *J. Fluid Mech.*, **148**, 1(1984).
5 Dandy, D. S. and Leal, L. G., *J. Fluid Mech.*, **208**, 161(1989).
6 Ryskin, G. and Leal, L. G., *J. Comput. Phys.*, **50**, 71 (1983).
7 Patankar, S. V., *Numerical Heat Transfer and Fluid Flow*, John Wiley, New York (1980).
8 Leonard, B. P., *Comput. Methods Appl. Mech. Eng.*, **12**, 59 (1979).
9 Pollard, A. and Siu, A. L. W., *Comput. Methods Appl. Mech. Eng.*, **35**, 293(1982).
10 Wasden, F. K. and Dukler, A. E., *AIChE J.*, **35**, 187(1989).
11 Mao, Z. Sh. and Dukler, A. E., *J. Comput. Phys.*, **91**, 132(1990).
12 Jenson, V. G., *Proc. Roy. Soc. Ser. A*, **249** (1256), 346(1959).
13 Rimon, Y. and Cheng, S. I., *Phys. Fluids*, **12**, 949 (1969).
14 Nakabayashi, K., Miyake, Y. and Aoi, T., *Nippon Kikai Gakkai Ronbushu, B-hen* (in Japanese) **51**(472), 4208(1985).
15 Taneda, S., *J. Phys. Soc. Japan*, **11**, 1104(1959).